# Viscous Interaction or Support Interference—The Dynamicist's Dilemma

Lars E. Ericsson* and J. Peter Reding†
*Lockheed Missiles & Space Company, Inc., Sunnyvale, Calif.*

**In hypersonic low-density flows, slender vehicle dynamics are affected by various viscous flow phenomena. The true viscid-inviscid interaction is often difficult to extract from the background of support interference in wind tunnel tests and nonlinear six-degree-of-freedom motion effects in ballistic range tests, as was demonstrated by Welsh, Winchenbach, and Madagan several years ago. The range data and wind tunnel results for a 10-deg cone were shown to give completely different $M_\infty$ trends for the pitch damping derivative. The aim of the present paper is to resolve this ambiguity and to help the vehicle designer decide how to obtain the best possible information about the full-scale vehicle dynamics using subscale dynamic test data.**

## Nomenclature

$c$ = reference length (maximum body diameter)
CG = $1-\Delta\bar{x}/\ell$, %
$d$ = body diameter
$\ell$ = sharp cone length (Fig. 10)
$l_S$ = sting length (Fig. 3)
$M$ = Mach number
$M_p$ = pitching moment, coefficient $C_m = M_p/\rho_\infty U_\infty^2/2)Sc$
$p$ = static pressure
$q$ = pitch rate
$Re$ = Reynolds number, $Re_x = xU_e/\nu_e$; $Re_{\ell\infty} = \ell_\infty U_\infty/\nu_\infty$
$S$ = reference area, $S=\pi c^2/4$
$t$ = time
$U$ = axial velocity (along wind axis)
$\Delta\bar{x}$ = axial body coordinate (see Fig. 10)
$\alpha$ = angle of attack
$\alpha_0$ = trim angle of attack
$\bar{\alpha}$ = angle-of-attack envelope, $\bar{\alpha} = |\alpha_0+\theta|_{\max}$
$\delta_S$ = sting deflection angle (Fig. 5)
$\Delta$ = increment and amplitude
$\theta$ = perturbation in pitch
$\Delta\theta$ = pitch amplitude
$\theta_c$ = cone half-angle (Fig. 10)
$\mu$ = viscosity
$\nu$ = kinematic viscosity, $\nu=\mu/\rho$
$\rho$ = density
$\omega,\bar{\omega}$ = circular frequency, $\bar{\omega}=\omega c/U_\infty$

*Subscripts*

$B$ = base
$d$ = discontinuity
$h$ = hysteresis
$N$ = nose
$S$ = sting
$\infty$ = freestream conditions

*Superscript*

$i$ = induced, e.g., due to wake and sting interactions

*Derivative Symbols*

$\dot{\theta}$ = $\partial\theta/\partial t$
$C_{m\alpha}$ = $\partial C_m/\partial\alpha$
$C_{mq}+C_{m\dot{\alpha}}$ = $C_{m\dot{\theta}} = \partial C_m \Big/ \partial\left(\frac{c\dot{\theta}}{U_\infty}\right)$
$C_{m\bar{\theta}}, C_{m\bar{\dot{\theta}}}$ = integrated mean coefficients for nonlinear characteristics

Presented as Paper 77-78 at the AIAA 15th Aerospace Sciences Meeting, Los Angeles, Calif., Jan. 24-26, 1977; submitted Feb. 10, 1977; revision received Oct. 21, 1977. 

Index categories: Entry Vehicle Testing, Flight and Ground; Nonsteady Aerodynamics; Jets, Wakes, and Viscid-Inviscid Flow Interactions.

*Consulting Engineer. Associate Fellow AIAA.
†Research Specialist. Member AIAA.

## Introduction

IT is well known that viscous interaction effects are important in hypersonic low-density flows. The problem is for the dynamicist to determine from his theoretical and experimental information what the true full-scale flight dynamics will be. Figure 1 illustrates his dilemma. It shows the experimental results compiled by Welsh et al.[1] for a 10-deg sharp cone, as well as some more recent test data.[2] Also shown are the inviscid flow results from Brong's theory.[3] The large influence of Mach number is to be expected, as the viscous interaction effects increase strongly with increasing Mach number. In Fig. 1, conventional wind tunnel test results, as well as ballistic range data, indicate that the viscous effect is slightly destabilizing statically. The dynamic stability data from the ballistic range show a strong damping increase with increasing Mach number relative to Brong's inviscid

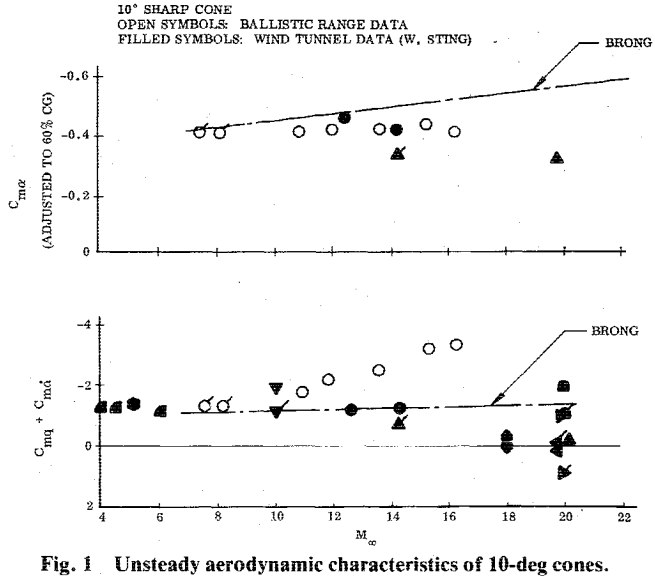


**Fig. 1 Unsteady aerodynamic characteristics of 10-deg cones.**

**Table 1 Test conditions for data in Fig. 1**

| Symbol | Facility | Reference | $Re_{l\infty} \times 10^6$ | $d_N/d_B$ | CG, % | $\bar{\omega}$ | $\bar{\alpha}$, deg |
|---|---|---|---|---|---|---|---|
| ○ | Ballistic range | 1 | 0.4 | .03-.07 | 63 | .004 | $2.5<\bar{\alpha}<12$ |
| ○ | Ballistic range | 1 | 0.4 | .03-.07 | 63 | .004 | $\bar{\alpha}<2.5$ |
| ▰ | Wind tunnel | 7 | 0.8 | 0 | 64 | .010 | $\bar{\alpha}>2$ |
| ⬢ | Wind tunnel | 2 | 9.0 | .07 | 67 | .008 | 2 |
| ▼ | Wind tunnel | 2 | 0.5 | .07 | 67 | .006 | 2 |
| ▲ | Wind tunnel | 2 | 0.5 | .017 | 67 | .006 | 2 |
| ● | Wind tunnel | 4 | 0.6 | 0 | 60 | .005 | $\bar{\alpha}\leq 2$ |
| ▼ | Wind tunnel | 5 | 0.25 | .017 | 59 | .005 | 1.5 |
| ▼ | Wind tunnel | 5 | 0.25 | .017 | 59 | .025 | 1.5 |
| ■ | Wind tunnel | 5 | 0.25 | .017 | 55 | .046 | 2 |
| ■ | Wind tunnel | 5 | 1.2 | .017 | 55 | .062 | 2 |
| ◆ | Wind tunnel | 5 | 0.56 | .017 | 55 | .023 | 1.75 |
| ▲ | Wind tunnel | 5 | 0.17 | .017 | 55 | .023 | 1.75 |
| ◀ | Wind tunnel | 6 | 0.28 | .017 | 59 | .004 | 1.5 |
| ◀ | Wind tunnel | 6 | 0.28 | .017 | 59 | .021 | 1.5 |
| ▶ | Wind tunnel | 6 | 0.14 | .017 | 59 | .004 | 1.5 |
| ▶ | Wind tunnel | 6 | 0.14 | .017 | 59 | .021 | 1.5 |

theory; however, the wind tunnel results show the opposite trend, i.e., a strong reduction of the damping leading to dynamic instability for high Mach numbers. The pertinent information in regard to test conditions, center of gravity, etc., for the test data[1,2,4-7] in Fig. 1 is given in Table 1.

The question the design engineer asks himself is, of course, "What are the full-scale characteristics going to be?" It is known that the wind tunnel data are subject to model support interference and sting plunging effects, whereas the ballistic range data may be difficult to interpret because of multi-degree-of-freedom vehicle motion, nonlinear amplitude effects, possible nose bluntening, and transient Mach number phenomena due to high deceleration of very light models. The aim of the present paper is to present information that will help the designer decide how to solve his dilemma.

## Discussion

The wind tunnel data[2,4-7] in Fig. 1 were obtained in the usual manner using a sting-supported model. It is well known that the interference from the sting support can be large, especially in regard to hypersonic dynamic stability data.[8] Figure 2 shows the large undamping interference from an asymmetric sting flare.[8] The near-zero damping derivatives in Fig. 1 for $M_\infty \approx 20$ belong to the set of data discussed by Hobbs in Ref. 9, and are definitely subject to asymmetric flared-sting interference[8,10] (see Fig. 2a). Comparing this hypersonic, asymmetric flared-sting interference with that documented for bulbous-based bodies at subsonic speeds[11,12] (see Fig. 2b), one comes to the conclusion that, at hypersonic speeds, even flat-based slender bodies can be subject to sting interference, a fact that was first demonstrated by Walchner et al. several years ago[13,14] (see Fig. 3). The asymmetric sting-strut juncture causes divergent oscillation of a sharp (0.39% nose bluntness) slender cone. Only when the distance between model base and sting-strut juncture was increased from 1.2 to 4.2 base diameters were the expected damped oscillations obtained. The highly nonlinear character of the damping coefficient in the presence of sting interference shown in Fig. 2 is typical.[8]

## Sting Interference

Further study of the high-Mach-number data[6] ($M_\infty \geq 20$) reveals some peculiar trends (Fig. 4). The data obtained with the stiff flexure show increasing damping with decreasing Reynolds number, whereas the data obtained with a soft flexure show decreased damping in agreement with what is predicted by local dynamic viscid-inviscid interaction theory[15] (Fig. 4a). According to theory[15] there is no effect of frequency for the range shown in Fig. 4a, i.e., for $\bar{\omega}^2 \ll 1$. Figure 4b shows how the frequency effect decreases with increasing Reynolds number (and associated dynamic pressure) until it has disappeared at $Re_{l\infty} \approx 0.3 \times 10^6$. This might suggest that the data trend in Fig. 4 was caused by mechanical support damping that was not adequately accounted for. However, the frequency trend goes the wrong way. It can be shown[16,17] that the tare damping would increase with decreasing frequency, a trend opposite to that displayed by the low-frequency data in Fig. 4.

Based upon the similarity shown in Fig. 2, the bulbous-base results[11,12] will be used to explore the possible sting interference effect in Fig. 4. Figure 5 shows the combined effects of sting deflection $\delta_S$ and angle of attack $\alpha$ on the pitching moment.[11,12] The "wake flipping" causes a highly nonlinear moment change that can be represented by a discontinuity $\Delta^i C_m$ for finite-amplitude oscillations. Note that for one-degree-amplitude oscillation ($\Delta\theta = 1$ deg), at $\alpha = 0$, $\delta_S$ in Fig. 5 varies from $\delta_S = -1$ deg to $\delta_S = 1$ deg. Thus the sting-induced increment $|\Delta^i C_m|$, which is several times as large as the aerodynamic moment $|C_{m_\alpha}\Delta\theta|$, will be included in the measurements. The corresponding integrated effect $\Delta^i C_{m\bar{\theta}}$ on the pitch damping derivative can be written

$$\Delta^i C_{m\bar{\theta}} = (\Delta^i C_{m\bar{\theta}})_d + (\Delta^i C_{m\bar{\theta}})_h \qquad (1)$$

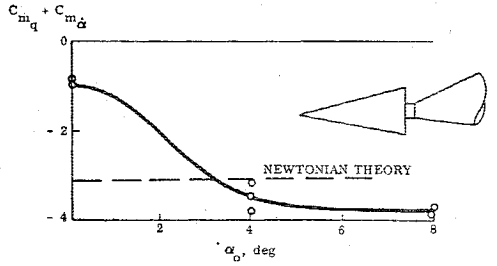


a) $M_\infty = 20.2$, $\Delta\theta = 3$ deg, $\theta_c = 10$ deg

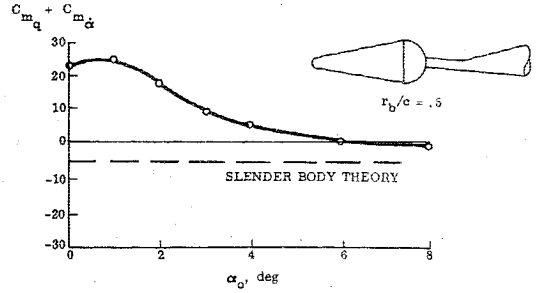


b) $M_\infty = 0.9$, $\Delta\theta = 1$ deg, $\theta_c = 6$ deg

**Fig. 2 Sting interference effects.**

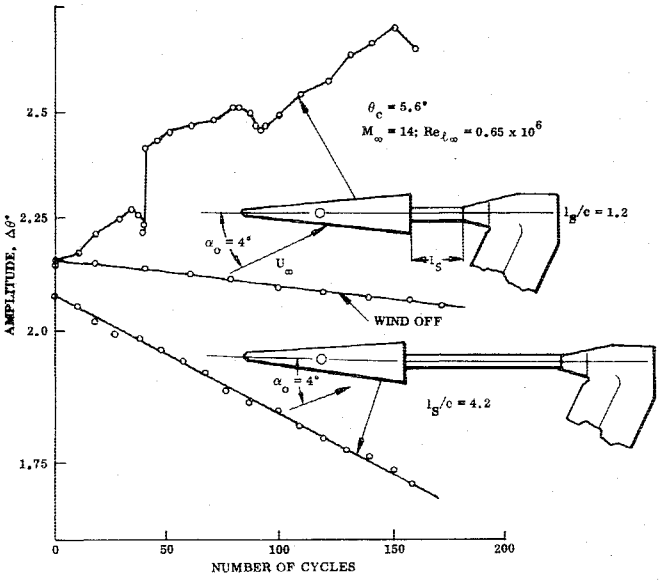


**Fig. 3 Strut interference effect on pitch damping.[14]**

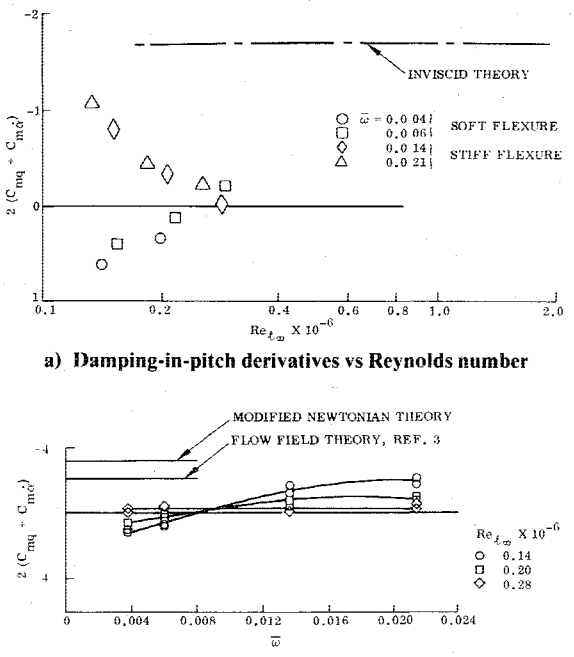


**a) Damping-in-pitch derivatives vs Reynolds number**




**b) Damping-in-pitch derivatives vs reduced frequency parameter**

**Fig. 4 Nonlinear sting interference.[6]**

where

$$\Delta^i C_{m\dot{\theta}d} = -\frac{2}{\pi}\frac{\Delta^i C_m}{\Delta\theta}\cdot\frac{U_\infty \Delta t}{c} \tag{2}$$

and

$$\Delta^i C_{m\dot{\theta}h} = -\frac{2}{\pi}\frac{\Delta^i C_m}{\Delta\theta}\cdot\frac{1}{\bar{\omega}}\frac{\Delta\alpha_h}{\Delta\theta} \tag{3}$$

where $\Delta t$ and $\Delta\alpha_h$ are the lumped representations of the time lag and hysteresis effects.[12] Figure 5 shows that the moment jump is stabilizing, $\Delta^i C_m < 0$. Thus according to the expressions above, both sting-induced effects are undamping $\Delta^i C_{m\dot{\theta}} > 0$. The pure discontinuity effect, Eq. (2), is inversely proportional to the amplitude $\Delta\theta$, whereas the hysteresis effect, Eq. (3), is inversely proportional to both amplitude and reduced frequency $\bar{\omega}$. Applying this formulation to the data in Fig. 4, trying to find a curve for zero hysteresis from

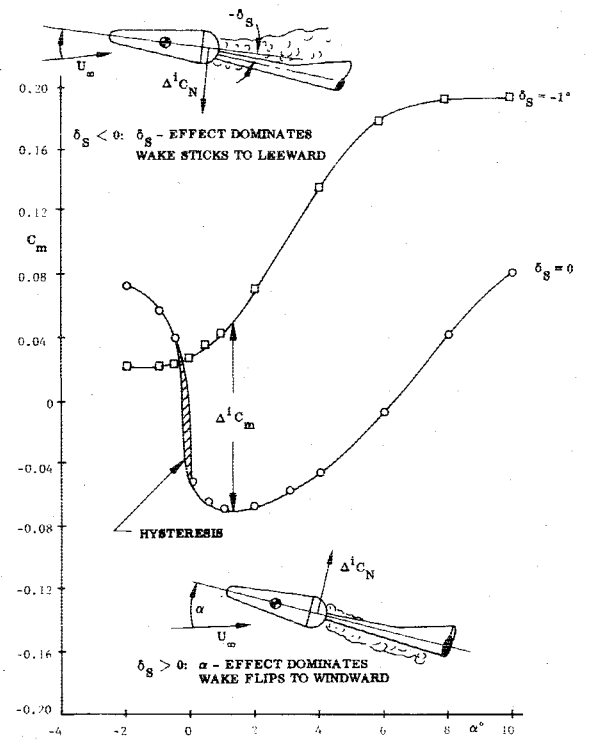


**Fig. 5 Nonlinear sting interferences with hysteresis.**

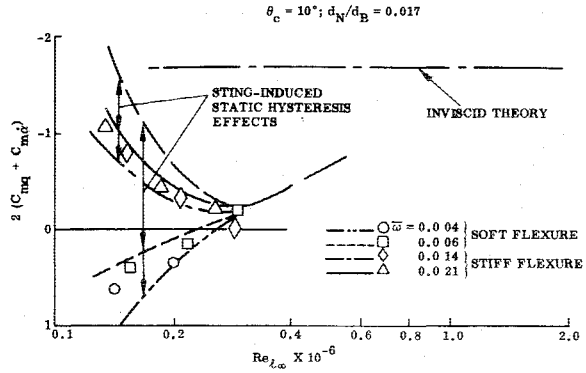


**Fig. 6 Combined effects of aerodynamic discontinuity and hysteresis on dynamic sting interference.**

which the frequency effects given by Eq. (3) would fit the data, gives the results shown in Fig. 6. That is, the frequency trend could be explained with asymmetric flared-sting interference of the type observed on bulbous-based bodies at subsonic speeds. Looking at Hama's flow pictures,[18] with the lip shock extending almost horizontally from the flat base, one can see a certain similarity between the base flow recirculation geometrics in the two cases, i.e., the flat base in hypersonic flow and the bulbous base in subsonic flow. Further credence to this postulated sting interference mechanism is given by Walchner's results.[13,14] Figure 7 shows the observed discontinuity and hysteresis in the base pressure variation with angle of attack. The divergent oscillation, indicating negative aerodynamic damping obtained for $l_S/c = 1.2$, is shown in the top trace of Fig. 3. It should be noted that only when the asymmetric flare-strut juncture was supplied with a splitter-plate fairing was the asymmetric sting interference on the base pressure eliminated completely, even for the long sting, $l_S/c = 4.2$ (Fig. 7b). This would indicate that, in hypersonic tests with a bulbous-based body, one would have to be particularly careful in regard to the support design. Using a symmetric sting-strut geometry, as is done at NAE,[19] is of course helpful in eliminating asymmetric sting-

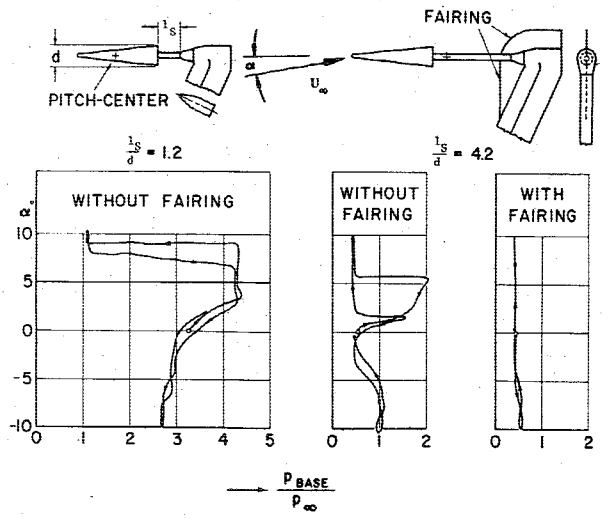


Fig. 7 Support effect on base pressure.[13]

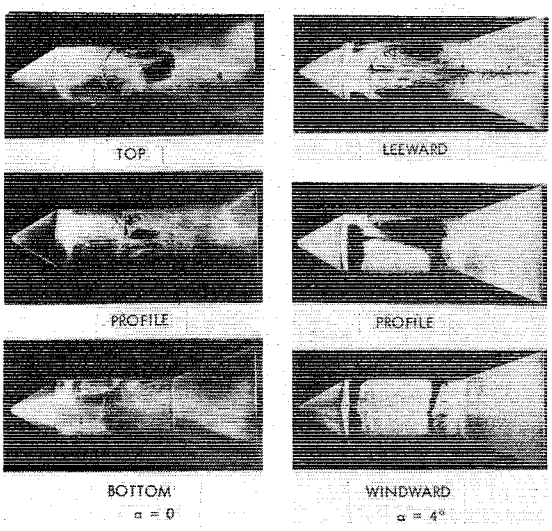


a) China clay flow patterns

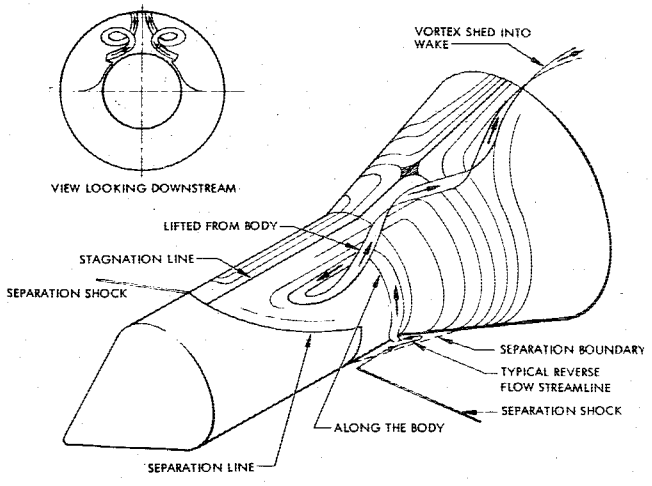


b) Deduced imbedded separated flow vortex

Fig. 8 Flare-induced separated flow patterns at $M_\infty = 1.2$.

flare interference. However, careful design is still needed to avoid symmetric sting( – flare) interference.[8]

Other peculiar frequency effects have been observed that cannot be explained by the hysteretic sting-flare interference discussed above. Uselton and Uselton[20] show such results for turbulent flow when a large symmetric sting flare, of the same diameter as the model base, was placed close to the base ($l_S/c = 1$). Similar odd frequency effects have been observed by LaBerge and Orlik-Rückemann[21] in "two-dimensional" dynamic tests of sharp wedges. In both of these cases one knows that large-scale vortices are present, generated by the wedge-sideplate corner flow in the "two-dimensional" case,[22-24] and by crossflow effects in the three-dimensional case. There is a breakdown of axisymmetry for the base flow on a slender cone at angle of attack, and one can expect that large-scale vortices will develop in the body wake much earlier than the so-called free body vortices.[25] The case of a slender cone followed by a large sting-flare is somewhat analogous to the separated flow geometry existing on a blunt cylinder-flare at transonic speeds[26] (Fig. 8). Thus, one can expect a dramatic change in separated flow pattern from the symmetric case at $\alpha = 0$ to the asymmetric case at $\alpha \neq 0$. This explains the discontinuous nature of the asymmetric sting-flare characteristics dicsussed earlier, as well as the possible vortex interference with the sting-flare (see Fig. 8b).

It is clear from the results discussed so far that in order to avoid, or at least minimize, aerodynamic sting interference effects, a rather long separation distance between model base and sting-flare has to be used ($l_S/c > 4$). Furthermore, in order to avoid cylindrical sting interference[8] the sting diameter has to be rather small. Both these requirements bring in another problem—that of sting plunging. This is, however, a less formidable problem than that of aerodynamic sting interference. The coupled pitch-plunge motion can be analyzed relatively simply.[27]

In ballistic range tests the six-degree-of-freedom motion causes great difficulties in regard to the data reduction, especially when the vehicle aerodynamics are highly nonlinear. Presently, when curve-fitting the vehcile motion data, a certain type of nonlinearity is usually postulated based upon computational expediency rather than on physical facts. Thus, it is difficult to obtain completely unbiased information about the nonlinear aerodynamics from free flight tests. Even in the simple case of planar motion, as observed in free flight or prescribed in free oscillation wind tunnel tests, it is difficult to obtain a true appreciation for the degree of nonlinearity. This is especially true for the dynamic characteristics. Figure 9 illustrates this for the case of nose-bluntness-induced nonlinear aerodynamics.[28] The finite-amplitude damping coefficient $C_{m\dot{\theta}} = f(\Delta\theta)$ for oscillations around $\alpha = 0$ is weighted by the square of the pitch rate, which is maximum at $\bar{\alpha} = 0$ and zero at $\bar{\alpha} = \Delta\theta$. This explains the slow response of the large-amplitude damping coefficient $C_{m\dot{\theta}} = f(\Delta\theta)$ to the highly nonlinear infinitesimal amplitude derivative $C_{m\dot{\theta}} = f(\alpha)$. Another purpose for introducing Fig. 9 here is to illustrate that $\bar{\alpha}$ has to extend far into the nonlinear region before the large-amplitude damping coefficient $C_{m\dot{\theta}}$ will show any effects. The figure also illustrates the fact that detailed information about nonlinear unsteady aerodynamics can only be obtained under the controlled conditions provided by small-amplitude oscillation tests in wind tunnels covering the angle-of-attack range of interest.

Another problem in ballistic range tests is that of nose bluntening. It is noted in Ref. 1 that the 10-deg cones might increase their bluntness from the initial value of 3.2% to 7% towards the end of the run. Figure 10 and Ref. 28 show that this bluntening would cause a 10% decrease in the dynamic stability derivative $C_{m\dot{\theta}}$, i.e., a trend opposite to the damping increase over inviscid theory shown in Fig. 1. It is shown in Ref. 29 that the effect of angle of attack can, in a first approximation, be accounted for by including $\alpha$ in the windward side effective tangent cone angle $(\theta_c + 8\alpha/3\pi)$. For the 7% blunt 10-deg cone, Fig. 10 shows that increasing the angle of attack from $\alpha = 0$ deg to $\alpha = 10$ deg would cause a damping increase of 10%. That is, for the ballistic range data in Fig. 1 with $\bar{\alpha} > 2.5$ deg, it appears that bluntening and attitude-amplitude effects would cancel each other, indicating that the

increased damping with increasing Mach number probably is a viscous flow effect.

## Viscid-Inviscid Interaction

The observant reader has probably already noticed a distinguishing characteristic of the high-Mach-number ballistic range data obtained by Welsh et al.[1]; i.e., it was obtained at high flow inclination, $\bar{\alpha} > 2.5$ deg, whereas the rest of the data in Fig. 1 is for $\bar{\alpha} < 2.5$ deg. It is therefore indicated that the increased damping may be caused by the dynamic effects of large viscous crossflow. This can be shown to be the case. For the data in Fig. 1 with CG in the neighborhood of 60% and $\bar{\alpha} > 2.5$ deg the dominant viscous-induced forces are caused by the leeside boundary-layer "hump" sketched in Fig. 11. The regular boundary-layer shear layer is lifted by a low-velocity inner layer generated by upstream crossflow effects. Because of the low velocity the convective time lag for the crossflow effects is large. Thus, the viscous-induced effect is to decrease static stability slightly and to increase dynamic stability greatly, similar to the effects of boundary-layer transition.[30,31] Using the aerodynamic static data obtained at $M_\infty = 7.95$ by Tracy,[32] the prediction shown in Fig. 12 was obtained. The computed viscous effect was applied in two ways to Brong's theoretical inviscid results—either added algebraically or applied as a correction factor—resulting in the data spread indicated by the crosshatched region. The agreement between prediction and experiment is very satisfactory. These large viscous crossflow effects will have important impact on pitch-yaw-roll coupling of slender reentry vehicles, especially in presence of ablation, and may figure prominently in any explanation of the observed pretransition behavior at Earth re-entry.

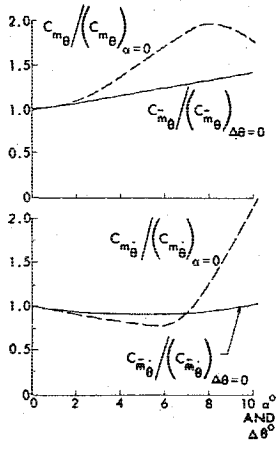


**Fig. 9 Comparison between infinitesimal and finite-amplitude stability derivatives: $\theta_c = 10$ deg, $d_N/d_B = 0.030$, $\Delta\bar{x}/$**

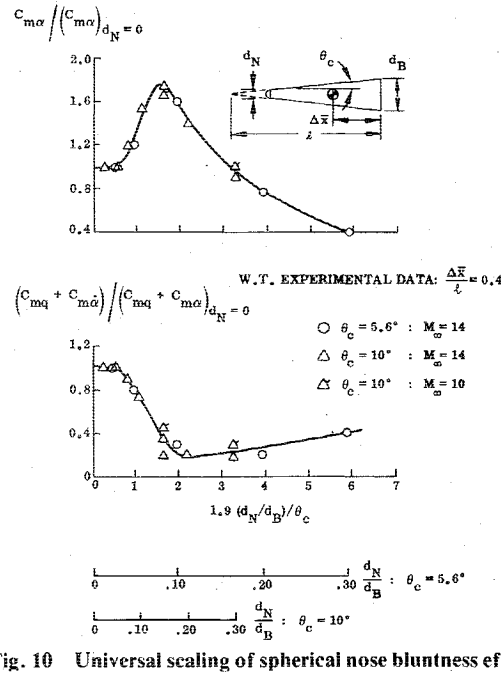


**Fig. 10 Universal scaling of spherical nose bluntness effects.**

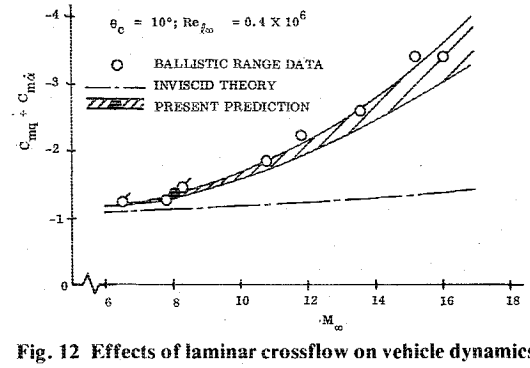


**Fig. 12 Effects of laminar crossflow on vehicle dynamics.**

## Conclusions

A thorough review of available theoretical and experimental information about the effects of viscous interaction and support interference on the hypersonic unsteady aerodynamics of slender cones has revealed the following.

1) The large increase of damping with increasing Mach number measured in a ballistic range by Welsh et al.[1] is a true viscous interaction effect caused by large laminar crossflow.

2) Support interference is a problem that is aggravated at increasing Mach numbers and by asymmetric sting-strut arrangements. It is often difficult to eliminate aerodynamic sting interference completely. However, it can be minimized through careful design until it is of little practical significance, as has been demonstrated by Walchner.

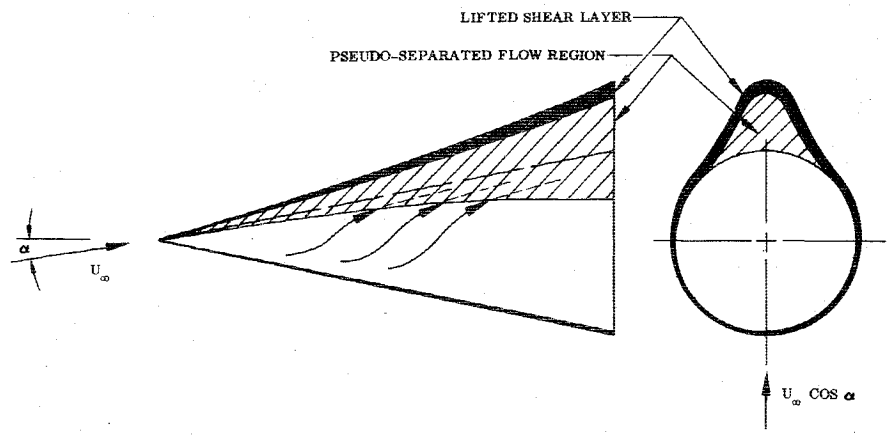


**Fig. 11 Laminar crossflow at $\alpha/\theta_c > 0.25$.**

## References

[1] Welsh, C. J., Winchenbach, G. L., and Madagan, A. N., "Free-Flight Investigation of the Aerodynamic Characteristics of a Cone at High Mach Numbers," *AIAA Journal*, Vol. 8, Feb. 1970, pp. 294-300.

[2] Morrison, A. M., Holmes, J. E., and Lawrence, W. R., "An Investigation of the Damping in Pitch Characteristics of a Ten Degree Cone," White Oak Laboratory, Silver Spring, Md., NSWC/WOL/TR 75-84, June 1975.

[3] Brong, E. A., "The Unsteady Flow Field about a Right Circular Cone in Unsteady Flight," FDL-TDR-64-148, Jan. 1967.

[4] Walchner, O., Sawyer, F., Quinn, B., and Friberg, E., "Hypersonic Stability Derivatives for a Standard 10 Degree Cone," ARL 67-0099, May 1967.

[5] Urban, R. H., "A Dynamic Stability Balance for Hypervelocity (Hot-Shot) Tunnels," AEDC-TR-65-222, Oct. 1965.

[6] Urban, R. H. and Shanahan, R. J., "Dynamic Stability Characteristics of a 10-Deg. Cone at Mach Number 20," AEDC-TR-65-80, April 1965.

[7] Prislin, R. H., "High Amplitude Dynamic Stability Characteristics of Blunt 10-Degree Cones," Jet Propulsion Lab., Pasadena, Calif., TR-32-1012, Oct. 1966.

[8] Reding, J. P. and Ericsson, L. E., "Dynamic Support Interference," *Journal of Spacecraft and Rockets*, Vol. 9, July 1972, pp. 547-553.

[9] Hobbs, R. B. Jr., "Hypersonic Dynamic Stability, Part II, Conical Body Experimental Programs," FDL-TDR-64-149, Part II, Jan. 1967.

[10] Hobbs, R. B. Jr., "Private Communication of Sting Geometry," July 1968.

[11] Adcock, J. B., "Some Experimental Relations Between the Static and Dynamic Stability Characteristics of Sting-Mounted Cones with Bulbous Bases," *Transactions of the 3rd Technical Workshop on Dynamic Stability Problems*, Vol. II, NASA Ames RC, Moffett Field, Calif., Nov. 1968, Paper 5.

[12] Ericsson, L. E. and Reding, J. P., "Aerodynamic Effects of Bulbous Bases," NASA CR-1339, Aug. 1969.

[13] Walchner, O. and Clay, J. T., "Nose Bluntness Effects on the Stability Derivatives of Cones in Hypersonic Flow," *Transactions of the Second Technical Workshop on Dynamic Stability Testing*, Vol. 1, Arnold Engineering Development Center, Tullahoma, Tenn., April 1965, Paper 8.

[14] Walchner, O., private communication of unpublished data on hypersonic dynamic support interference, June 1968.

[15] Orlik-Rückemann, K. J., "Oscillating Slender Cone in Viscous Hypersonic Flow," *AIAA Journal*, Vol. 10, Sept. 1972, pp. 1139-1140.

[16] Welsh, C. J. and Ward, L. K., "Structural Damping in Dynamic Stability Testing," AEDC-TR-59-5, Feb. 1959.

[17] Schueler, C. J., Ward, L. K., and Hodapp, A. E. Jr., "Techniques for Measurement of Dynamic Stability Derivatives in Ground Test Facilities," AGARDograph 121, Oct. 1967.

[18] Hama, F. R., "Experimental Studies of the Lip Shock," *AIAA Journal*, Vol. 6, Feb. 1968, pp. 212-219.

[19] Orlik-Rückemann, K. J. and LaBerge, J. G., "Static and Dynamic Pitching Moment Measurements on a Family of Elliptic Cones at Mach Number 11 in Helium," National Research Council of Canada, NRC NAE LTR-VA-14, 1970.

[20] Uselton, J. C. and Uselton, B. L., "A Look at the Validity of the Small Amplitude Oscillation Dynamic-Stability Measurement Technique," *Journal of Spacecraft and Rockets*, Vol. 13, No. 5, May 1976, pp. 266-270.

[21] LaBerge, J. G. and Orlik-Rückemann, K. J., "Dynamic Stability Tests of Sharp Slender Wedges at $M=9$ and $M=18$ in Helium," NAE, Ottawa, Canada, Lab Memo. No. HG 2-29, (Preliminary Data), July 1968.

[22] Charwat, A. F. and Redekopp, L. G., "Supersonic Interference Flow Along the Corner of Intersecting Wedges," *AIAA Journal*, Vol. 5, March 1967, pp. 480-488.

[23] Korkegi, R. H., "Survey of Viscous Interactions Associated with High Mach Number Flight," *AIAA Journal*, Vol. 9, May 1971, pp. 771-784.

[24] Watson, R. D. and Weinstein, L. M., "A Study of Hypersonic Corner Flow Interactions," *AIAA Journal*, Vol. 9, No. 7, July 1971, pp. 1280-1286.

[25] Rainbird, W. J., "Turbulent Boundary-Layer Growth and Separation on a Yawed Cone," *AIAA Journal*, Vol. 6, Dec. 1968, pp. 2410-2416.

[26] Reding, J. P., Guenther, R. A., Ericsson, L. E., and Leff, A. D., "Nonexistence of Axisymmetric Separated Flow," *AIAA Journal*, Vol. 7, July 1969, pp. 1374-1375.

[27] Ericsson, L. E., "Effect of Sting Stiffness on Measured Derivatives for a Model Describing Pitch Oscillations of Low Reduced Frequency," Lockheed Missiles & Space Company, Sunnyvale, Calif., DP/M-TM-27, Dec. 1960; see also Appendix of AIAA Paper 77-78, Jan. 1977.

[28] Ericsson, L. E., "Unsteady Embedded Newtonian Flow," *Astronautica Acta*, Vol. 18, Nov. 1973, pp. 309-330.

[29] Ericsson, L. E., "Universal Scaling Laws for Hypersonic Nose Bluntness Effects," *AIAA Journal*, Vol. 7, Dec. 1969, pp. 2222-2227.

[30] Ericsson, L. E., "Effect of Boundary Layer Transition on Vehicle Dynamics," *Journal of Spacecraft and Rockets*, Vol. 6, Dec. 1969, pp. 1404-1409.

[31] Ericsson, L. E., "Transition Effects on Slender Vehicle Stability and Trim Characteristics," *Journal of Spacecraft and Rockets*, Vol. 11, Jan. 1974, pp. 3-11.

[32] Tracy, R. C., "Hypersonic Flow over a Yawed Circular Cone," California Institute of Technology, Pasadena, Calif., CIT/GAL Memo No. 69, Aug. 1963.